The Astrophysical Journal Letters, 922:L38 (8pp), 2021 December 1 https://doi.org/10.3847/2041-8213/ac399d

Internal-current Lorentz-force Heating of Astrophysical Objects

Christopher F. Chyba[1,2] and Kevin P. Hand[3]
[1] Department of Astrophysical Sciences, Princeton University, 4 Ivy Lane, Princeton, NJ 08544, USA; cchyba@princeton.edu
[2] Princeton School of Public and International Affairs, Princeton University, 221 Nassau Street, Princeton, NJ 08544, USA
[3] Jet Propulsion Laboratory, California Institute of Technology, Pasadena, CA 91109, USA
Received 2021 August 8; revised 2021 November 13; accepted 2021 November 14; published 2021 December 1

Abstract

Two forms of ohmic heating of astrophysical secondaries have received particular attention: unipolar-generator heating with currents running between the primary and secondary, and magnetic induction heating due to the primary's time-varying field. Neither appears to cause significant dissipation in the contemporary solar system. But these discussions have overlooked heating derived from the spatial variation of the primary's field across the interior of the secondary. This leads to Lorentz-force-driven currents around paths entirely internal to the secondary, with resulting ohmic heating. We examine three ways to drive such currents, by the cross product of (1) the secondary's azimuthal orbital velocity with the nonaxially symmetric field of the primary, (2) the radial velocity (due to nonzero eccentricity) of the secondary with the primary's field, or (3) the out-of-plane velocity (due to nonzero inclination) with the primary's field. The first of these operates even for a spin-locked secondary whose orbit has zero eccentricity, in strong contrast to tidal dissipation. We show that Jupiter's moon Io today could dissipate about 600 GW (more than likely current radiogenic heating) in the outer 100 m of its metallic core by this mechanism. Had Io ever been at 3 Jovian radii instead of its current 5.9, it could have been dissipating 15,000 GW. Ohmic dissipation provides a mechanism that could operate in any solar system to drive inward migration of secondaries that then necessarily comes to a halt upon reaching a sufficiently close distance to the primary.

Unified Astronomy Thesaurus concepts: Natural satellite dynamics (2212); Natural satellites (Solar system) (1089); Magnetic fields (994); Io (2190); Jovian satellites (872); Exoplanet dynamics (490); Orbital evolution (1178); Triton (2187)

1. Introduction

Two forms of ohmic (Joule) heating of astrophysical objects have been emphasized in the literature. The first, viewed in the reference frame of the rotating primary, is an analog to Lorentz-force-driven current flow and the resulting ohmic dissipation in the Faraday disk (Faraday 1832; Munley 2004; Chyba et al. 2015). Such unipolar heating has been explored as a dissipation mechanism for Jupiter's moons Io (Piddington & Drake 1968; Goldreich & Lynden-Bell 1969; Drobyshevski 1979; Colburn 1980) and Europa (Reynolds et al. 1983; Colburn & Reynolds 1985), and Saturn's moon Enceladus (Hand et al. 2011). It has also been considered for planetesimal heating by the T-Tauri Sun (Sonnet et al. 1970), and for astrophysical binary systems (Laine & Lin 2012). In the planetary-satellite instantiation of this hypothesis, current flows in the ionosphere of the primary, down a flux tube to the primary-facing equatorial region of the secondary, through the conducting secondary, and then back to the primary. But in the case of Jupiter's moon Io, the plasma likely shunts the circuit around Io itself, resulting in little internal Joule heating (Colburn 1980; Goertz 1980; Russell & Huddleston 2000; Saur et al. 2004). At Europa, the current is limited by the resistance of the ice shell overlying the conducting ocean; significant heating would require connecting the circuit to the ocean through cracks in the ice (Reynolds et al. 1983; Colburn & Reynolds 1985), a possibility that should be reexamined now that possible plumes at Europa have apparently been observed (Roth et al. 2014; Sparks et al. 2016). At Enceladus, currents may be able to do just this, flowing through the "tiger stripes" at the south pole, but even so the resulting Joule heating would provide $<1\%$ of the observed heat flux (Hand et al. 2011).

A second form of ohmic heating featured in the literature is magnetic induction heating due to eddy (Foucault) currents driven by the primary's time-varying magnetic field. Seen in the frame of the rotating (likely spin-locked) secondary, the primary's field varies with time due to the primary's rotation if there are off-axis components of its magnetic flux density $\boldsymbol{B}$, or to variations in the field experienced by the secondary as it moves in an eccentric or inclined orbit. This model in effect treats the secondary as sitting in the interior field of a giant solenoid with spatially constant but temporally oscillating $\boldsymbol{B}$. We have presented analytical induction-heating formulae for each of these cases, and find that such heating appears negligible for satellites in our solar system (Chyba et al. 2021). In the case of highly conducting spheres (such as for Fe or Fe–S cores of satellites), total heating is limited because the oscillating magnetic field penetrates only about one skin depth δ into the conductor. For Fe or Fe–S cores of Io or Europa, for example, $\delta \approx 100$ m, so nearly all of the core remains unheated. In the case of a low-conductivity spherical shell (perhaps a low-conductivity magma or liquid water ocean), the field can penetrate the conductor deeply, but then the inductive reactance becomes very large. This finding of insignificant induction heating for objects in our solar system is consistent with earlier conclusions based on numerical treatments or waveguide models for specific objects (Colburn 1980; Simonelli 1983; Khurana et al. 1998). Exoplanets close to certain types of host stars might experience significant induction heating, however (Laine et al. 2008; Kislyakova et al. 2017).

These discussions have overlooked an additional ohmic heating mechanism, one that derives from the spatial variation of the primary's field $\boldsymbol{B}$ through or across the interior of the secondary. (There is something of an analogy to tidal heating, which results from the variation of the primary's gravitational field through the secondary.) This leads to Lorentz-force-driven currents around paths entirely internal to the secondary, with resulting dissipation. Here we show that this effect can generate significant heating for at least one moon in our current solar system, and perhaps greater heating in the past. It seems likely that analogous dissipation occurs in objects in extrasolar systems as well.

2. A New Mechanism

The idea of this proposed mechanism can be seen by considering the fundamental definition of electromotive force (emf, or ε), viz. the work per unit charge done around a path C due to the Lorentz force (e.g., Scanlon et al. 1969):

$$\varepsilon = \oint_C (\boldsymbol{E} + \boldsymbol{v} \times \boldsymbol{B}) \cdot d\boldsymbol{l}. \tag{1}$$

Absent jump discontinuities (e.g., Auchmann et al. 2014) on the corresponding surface S this becomes, via Stokes' theorem and the Faraday-Maxwell equation,

$$\varepsilon = \int_S [-\partial \boldsymbol{B}/\partial t + \boldsymbol{\nabla} \times (\boldsymbol{v} \times \boldsymbol{B})] \cdot d\boldsymbol{a}. \tag{2}$$

We first work in a frame K rotating with the primary. Consider a secondary orbiting in the equatorial plane of its primary in a circular orbit. Take the secondary to be synchronously rotating (spin locked). Define coordinate systems with the usual conventions with origin at the center of the primary and z-axis along the primary's rotation axis. We then write the azimuthal velocity of the secondary as

$$\boldsymbol{v}_{\varphi} = v_{\varphi}\hat{\boldsymbol{\varphi}} = \omega r \sin\theta \hat{\boldsymbol{\varphi}}, \tag{3}$$

using spherical coordinates (r, θ, φ) with $\omega = \Omega - n$ the angular velocity of the secondary viewed from K, where Ω is the spin angular velocity of the primary and n is the secondary's mean motion. In K, $\partial \boldsymbol{B}/\partial t = \boldsymbol{0}$, and using $\boldsymbol{\nabla} \cdot \boldsymbol{B} = 0$ it is easy to show from Equation (3) that (Chyba & Hand 2016)

$$\begin{aligned} \boldsymbol{\nabla} \times (\boldsymbol{v}_{\varphi} \times \boldsymbol{B}) &= -\omega \left(\frac{\partial B_r}{\partial \varphi}\hat{r} + \frac{\partial B_{\theta}}{\partial \varphi}\hat{\theta} + \frac{\partial B_{\varphi}}{\partial \varphi}\hat{\varphi} \right) \\ &= -\omega \partial \boldsymbol{B}/\partial \varphi, \end{aligned} \tag{4}$$

which is $\boldsymbol{0}$ for any axially symmetric $\boldsymbol{B}$. Under these conditions, emf $= 0$ around *any* interior path C within the body of the secondary. So, for example, since Saturn's intrinsic magnetic field is azimuthally symmetric (Christensen et al. 2019), the $\boldsymbol{v} \times \boldsymbol{B}$ force cannot generate a nonzero emf around any interior path in a synchronously rotating satellite orbiting Saturn in a circular equatorial orbit. Similarly, the dipole, quadrupole, and octupole components of Jupiter's $\boldsymbol{B}$ field cannot generate an emf around any path in the interior of an analogous Jovian satellite. But Equation (4) also shows that an emf can be generated by those components of Jupiter's $\boldsymbol{B}$ field that vary azimuthally. Such components use the $\boldsymbol{v} \times \boldsymbol{B}$ force to drive purely internal currents, even for $\boldsymbol{v}$ given by Equation (3). The resulting energy dissipation (due to ohmic heating) operates even for spin-locked secondaries with obliquity and orbital eccentricity equal to zero. This contrasts with dissipative heating (and resulting orbital evolution) due to tidal effects: tidal dissipation within the secondary is zero for a spin-locked secondary in a circular orbit with zero obliquity (e.g., Chyba et al. 1989).

But what about charge redistribution within the orbiting body? We might expect the $\boldsymbol{v} \times \boldsymbol{B}$ force to drive electron redistribution until the resulting electrostatic field $\boldsymbol{E}$ perfectly cancels the $\boldsymbol{v} \times \boldsymbol{B}$ field, so that $\boldsymbol{E} = -\boldsymbol{v} \times \boldsymbol{B}$ everywhere within the conductor, guaranteeing emf $= 0$ in Equation (1). This is true for many simple examples of conductors moving through magnetic fields (Lorrain et al. 1998). The charge redistribution occurs extremely rapidly, on a classical relaxation timescale $\tau_e \sim \epsilon_0/\sigma \approx 10^{-11}$ (1 S m$^{-1}/\sigma$) s (Redžić 2004), where σ is electrical conductivity and ϵ_0 is vacuum permittivity. In highly conducting metals the relaxation time is given by the electron collision timescale $\tau_c \sim 10^7 \tau_e$, or $\sim 10^{-11}$ s (Gutmann & Borrego 1974). In either case, charge would seem to redistribute rapidly and continuously to maintain $\boldsymbol{E} = -\boldsymbol{v} \times \boldsymbol{B}$, so that emf $= 0$ by Equation (1) always. However, this argument fails when $\boldsymbol{\nabla} \times (\boldsymbol{v} \times \boldsymbol{B}) \neq \boldsymbol{0}$ (Chyba & Hand 2016, 2020), because the electric field of a static charge distribution may always be written as a potential of a scalar field: $\boldsymbol{E} = -\boldsymbol{\nabla} V$. But since $\boldsymbol{\nabla} \times \boldsymbol{\nabla} V = \boldsymbol{0}$ always, the equation $\boldsymbol{E} = -\nabla V = -\boldsymbol{v} \times \boldsymbol{B}$ can hold only if $\boldsymbol{\nabla} \times (\boldsymbol{v} \times \boldsymbol{B}) = 0$, which is violated in Equation (4) for any $\boldsymbol{B}$ that varies with φ. Charge redistribution cannot stop a current from flowing in this case. If $\boldsymbol{B}$ can be written as $\boldsymbol{B} = \boldsymbol{B_0} + B(\varphi)$, where $\boldsymbol{B_0}$ is independent of φ over S, electron redistribution will cancel the $\boldsymbol{v} \times \boldsymbol{B_0}$ component. But this has no effect on the emf, because this component would integrate to $\boldsymbol{0}$ around C in Equation (1) regardless.

Next we consider orbits for which $e \neq 0$. A secondary orbiting with $e \neq 0$ has a component of its velocity radially toward or away from its primary, varying with the true anomaly f around its orbit:

$$\boldsymbol{v_r} = v_r \hat{r} = nae(1 - e^2)^{-1/2} \sin f \ \hat{r}, \tag{5}$$

for semimajor axis a (Murray & Dermott 1999). Because this velocity varies with position around the secondary's elliptical orbit, and is independent of the primary's rotation, even in the frame K the relevant angular velocity is n, not ω. (One way to look at this is to imagine the special case of a primary with an axisymmetric field and a secondary in an eccentric orbit. The relevant frequency for, say, the skin depth in the secondary is n, no matter how fast or slow the primary is rotating.) We find

$$\begin{aligned} &\boldsymbol{\nabla} \times (\boldsymbol{v_r} \times \boldsymbol{B}) \\ &= \frac{v_r}{r}\left[\frac{1}{\sin\theta} \frac{\partial (B_{\theta} \sin\theta)}{\partial \theta}\hat{r} - \frac{\partial (rB_{\theta})}{\partial r}\hat{\theta} - \frac{\partial (rB_{\varphi})}{\partial r}\hat{\varphi} \right], \end{aligned} \tag{6}$$

so $\boldsymbol{v_r}$ can lead to emf generation even for axially symmetric primary $\boldsymbol{B}$ fields.

Finally we consider orbits for which inclination $i \neq 0$, and show that these orbits, too, can generate electrical heating via the axisymmetric dipole field (as well as, of course, via other components of the field). A satellite orbiting with $i \neq 0$ has a component of its velocity in the $\pm\hat{\theta}$ direction, varying with f around its orbit. We approximate this velocity by noting that at apoapse, the secondary is at a height $z = a(1 + e)\sin i$ above the primary's equatorial plane, whereas at periapse it is at a

height $z = -a(1 - e)\sin i$ below the plane. Therefore in one-half an orbital period the secondary moves a vertical distance of $2a \sin i$, giving it an average velocity in the $\hat{\theta}$ direction of

$$\boldsymbol{v}_{\boldsymbol{\theta}} = v_{\boldsymbol{\theta}}\hat{\boldsymbol{\theta}} = (2/\pi)na \sin i \, \hat{\boldsymbol{\theta}}. \tag{7}$$

Once again, the relevant angular velocity is n, not ω. We find

$$\boldsymbol{\nabla} \times (\boldsymbol{v}_{\boldsymbol{\theta}} \times \boldsymbol{B}) = \frac{v_\theta}{r}\left\{ -\frac{1}{\sin\theta}\frac{\partial(B_r \sin\theta)}{\partial\theta}\hat{r} + \left[\frac{1}{\sin\theta}\frac{\partial B_\varphi}{\partial\varphi} + \frac{\partial(rB_r)}{\partial r}\right]\hat{\theta} - \frac{\partial B_\varphi}{\partial\theta}\hat{\varphi}\right\}, \tag{8}$$

and an emf can be generated even if the primary field is axisymmetric.

All three cases considered here use the $\boldsymbol{v} \times \boldsymbol{B}$ part of the Lorentz force in K to drive currents around conducting paths entirely interior to the secondary. The power P dissipated in the secondary is then given by

$$P = \overline{\varepsilon^2}R/Z^2, \tag{9}$$

where $\overline{\varepsilon^2}$ is the square of the emf in Equation (1), averaged around one orbit, $Z = R + i\omega L$ is the conductor's impedance for the appropriate angular velocity , with

$$Z^2 = R^2 + (\omega L)^2, \tag{10}$$

and R and L are the conductor's resistance and inductance, respectively. (For the case of $\boldsymbol{v_r}$ or $\boldsymbol{v_\theta}$, ω in these expressions would be replced by n.) Values for R, L, and Z have been previously determined for conducting spheres and spherical shells (Chyba et al. 2021), geometries that roughly correspond to current paths in secondaries' metallic cores, or spherical shells of conducting magma or liquid water oceans.

3. Ohmic Heating for Conducting Spheres

We calculate the emf for the three cases considered here, on the assumption that the relevant part of the secondary in which current flows is a solid sphere (for example, a conducting Fe or Fe–FeS core of a planetary satellite). We consider spherical shells (for example, magma or liquid water oceans) in Section 4. We employ the usual magnetic field model for the primary field $\boldsymbol{B}$, in terms of Schmidt quasi-normalized associated Legendre polynomials with coefficients g_l^m and h_l^m of degree l and order m (e.g., Parkinson 1983; Merrill et al. 1998). Depending on the application, we make use of the primary field's axisymmetric components ($\boldsymbol{B}^{m=0}$; Appendix A), or its nonaxisymmetric components ($\boldsymbol{B}^{m\neq 0}$) through second order (Appendix B).

3.1. Azimuthal Velocities

We calculate the emf by Equation (2) in K for the case of azimuthal velocities $\boldsymbol{v}_{\varphi}$. In the frame K rotating with the primary, $\partial\boldsymbol{B}/\partial t = \boldsymbol{0}$ not only for the axisymmetric components but for the nonaxisymmetric components as well. Then we can obtain the emf by integrating $\boldsymbol{v}_{\varphi} \times \boldsymbol{B}$ around relevant current paths. The $\boldsymbol{B}^{m=0}$ components give $\boldsymbol{0}$ to all orders by Equation (4). To calculate the contribution of the $\boldsymbol{B}^{m\neq 0}$ components, we first examine more carefully the argument that $\partial\boldsymbol{B}/\partial t = \boldsymbol{0}$ in K. This certainly holds in frame K for any imaginary curve C orbiting the primary in empty space. However, consider the effects on the primary's field $\boldsymbol{B}$ at particular points in space as a conductor carrying C passes through those points during the conductor's orbit about the primary. Define the frame K' to be the frame that orbits and rotates with the secondary. In K', the secondary sees an oscillatory time dependence due to the nonaxisymmetric field, meaning that the nonaxisymmetric field must fall off exponentially into the conductor with an e-folding distance given by the skin depth

$$\delta = (2/\sigma\omega\mu)^{1/2}, \tag{11}$$

where we take magnetic permeability $\mu = \mu_0$ with $\mu_0 = 4\pi \times 10^{-7}$ H m^{-1} the permeability of free space. In general $\mu = \mu_r\mu_0$. Setting the relative permeability $\mu_r = 1$ is clearly the right choice for rock or ice, but is also likely the correct choice for a satellite's iron core, because $\mu_r = 1$ if the temperature of the core is above the Curie temperature $T_c = 1043$ K for iron, with little pressure dependence (Campbell 2003).

This same δ in Equation (11) must be present in K as well. For a planetary satellite, the relevant conducting sphere (of radius r_o) will presumably be made of Fe or Fe–FeS, for which $\sigma \sim 10^6$ S m^{-1} (Li et al. 2007; Silber et al. 2018), and we will have $\delta \ll r_o$. So even in K, $\boldsymbol{B}$ changes with time as the conducting sphere orbits, in effect shielding successive regions of space from the $\boldsymbol{B}^{m\neq 0}$ components of the field. However, this $\partial\boldsymbol{B}/\partial t \neq \boldsymbol{0}$ effect just drives the emf we have previously calculated from an induction-heating model in K' that treats $\boldsymbol{B}^{m\neq 0}$ as spatially constant but with a sinusoidal time dependence given by $\varphi = \omega t$ (Chyba et al. 2021). The emf in K equals the emf' in K' to within a factor $(v/c)^2 \sim 10^{-12}$ (Scanlon et al. 1969). For $\delta \ll r_o$, the induction model gives $\varepsilon = \omega B^{1,1} 2\pi r_o \delta$ to leading order, smaller than the emf values we find in Equations (14)–(16) by a factor $\sim\delta/r_o \sim 10^{-4}$, so its contribution to Equation (2) can be ignored.

Current paths C for our mechanism lie in the outermost-skin-depth layer of the conducting sphere of the secondary. Because of the skin-depth effect, $\boldsymbol{B}^{m\neq 0}$ at radius s in the conducting sphere of radius r_o falls off like $\boldsymbol{B}^{m\neq 0}(s) = \boldsymbol{B}^{m\neq 0}(r_o)\exp[-(r_o - s)/\delta]$ within the sphere. We employ a common approximation, treating $\boldsymbol{B}^{m\neq 0}$ to penetrate with no attenuation an outer layer of thickness δ of the conducting sphere and to be $\boldsymbol{0}$ further within (Wouch & Lord 1978; Chyba et al. 2021). An emf is generated around any path C (with line element $d\boldsymbol{l}$) in this outermost layer of the conducting secondary for which $\oint_C (\boldsymbol{v}_{\varphi} \times \boldsymbol{B}) \cdot d\boldsymbol{l} \neq 0$. By Equation (3), we have

$$\boldsymbol{v}_{\boldsymbol{\varphi}} \times \boldsymbol{B} = -v_\varphi B_\theta \hat{r} + v_\varphi B_r \hat{\theta}, \tag{12}$$

so there are three orientations of the current path C around which an emf may be driven: (a) paths in planes of constant r, extending from the nearside of the secondary to its farside, driven by the $\hat{\theta}$ term in Equation (12); (b) paths in planes of constant θ, driven by the $\hat{r}$ term in Equation (12); and (c) paths in planes of constant φ, driven by both terms of Equation (12). Ohmic heating results from currents running in each of these orthogonal sets of planes. Examples of these three paths are shown in Figure 1.

Using Equations (B1a)–(B3c), we calculate the emf for path orientations (a), (b), and (c) by Equation (1), integrating around a curve $\bar{C}$ that is the circumference of the average azimuthal current path of the relevant orientation in the conducting sphere

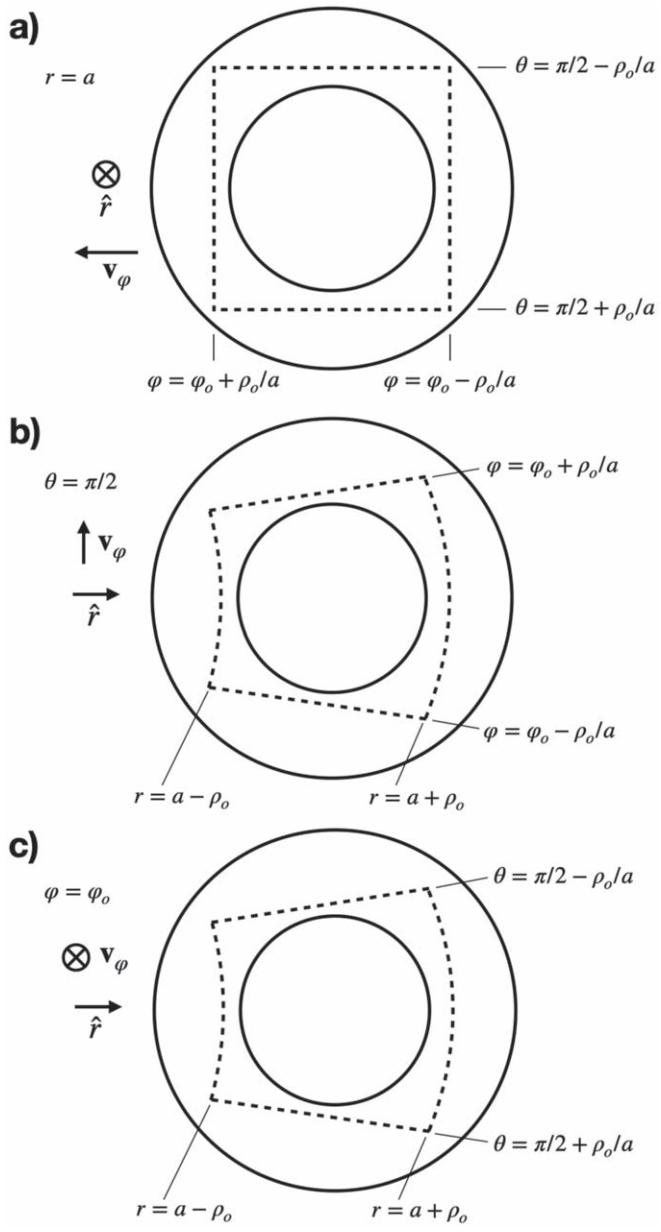

Figure 1. Integration paths (dotted lines) used to calculate the line integrals in Equations (14), (15), and (16). The paths lie in the outermost skin depth of the conducting sphere, represented here by showing the paths to lie between concentric circles of radii $\rho_o - \delta$ and ρ_o. The radius ρ_o, defined in Equation (13), is the radius corresponding to the average circumference for a current path for that orientation. In (a) segments are in the $\hat{\theta}$ and$\hat{\varphi}$ directions, in (b) the $\hat{r}$ and $\hat{\varphi}$ directions, and in (c) the $\hat{r}$ and $\hat{\theta}$ directions. Illustrations not to scale.

(of radius r_o) of the secondary, viz. $\bar{C} = \pi^2 r_o/2$ (Chyba et al. 2021), corresponding to an annular radius

$$\rho_o = \pi r_o/4. \tag{13}$$

To make Equation (1) analytically tractable, we choose paths of integration consisting of four legs, each leg locally parallel to $\hat{r}$, $\hat{\theta}$, or $\hat{\varphi}$; Figure 1(a) illustrates this path for case (a), with the radial line from the primary to the secondary lying in the $\theta = \pi/2$ plane and along some arbitrary value $\varphi = \varphi_o$, which will subsequently be averaged over 2π. Then by Equations (1), (3), (12), and (B1a)–(B3c), and with $d\boldsymbol{l} = \hat{r}dr + \hat{\theta}rd\theta + \hat{\varphi}r\sin\theta d\varphi$,

$$\varepsilon = \oint_{\bar{C}_a} v_\varphi B_r r d\theta \approx \frac{\pi^2}{2}\omega r_o^2\left(\frac{R_p}{a}\right)^3 \times \left[-g_1^1\sin\varphi_o + h_1^1\cos\varphi_o + \frac{3\sqrt{3}}{2}\left(\frac{R_p}{a}\right)(-g_2^2\sin 2\varphi_o + h_2^2\cos 2\varphi_o)\right], \tag{14}$$

where $v_\varphi B_2^1$ integrated to zero. Similarly (see Figure 1(b)), for cases (b) and (c) we find

$$\varepsilon = -\oint_{\bar{C}_b} v_\varphi B_\theta dr \approx -\frac{\pi^2\sqrt{3}}{4}\omega r_o^2 \times \left(\frac{R_p}{a}\right)^4 (g_2^1\sin\varphi_o - h_2^1\cos\varphi_o), \tag{15}$$

and (see Figure 1(c))

$$\varepsilon = \oint_{\bar{C}_c} v_\varphi(-B_\theta dr + B_r r d\theta) \approx \frac{\pi^2}{4}\omega r_o^2\left(\frac{R_p}{a}\right)^3 \times \left[g_1^1\cos\varphi_o + h_1^1\sin\varphi_o + 2\sqrt{3} \times \left(\frac{R_p}{a}\right)(g_2^2\cos 2\varphi_o + h_2^2\sin 2\varphi_o)\right]. \tag{16}$$

We sketch these calculations in Appendix C.

We now use Equations (9) and (10) to derive an expression for the power dissipated due to the emfs in Equations (14)–(16). The ohmic heating due to each path C_a, C_b, and C_c is separately calculated and the three are then summed for the total dissipation. For a conducting sphere with $r_o \gg \delta$, we have (Chyba et al. 2021)

$$R_{\text{sphere}} = \frac{\pi}{2\sigma\delta} \quad \text{and} \quad L_{\text{sphere}} = \frac{\pi\sqrt{3}}{4}\mu_0\delta, \tag{17}$$

so that by Equation (10), $Z^2_{\text{sphere}} = 4R^2_{\text{sphere}}$ and

$$\frac{R}{Z^2} = \frac{1}{\pi}\left(\frac{\sigma}{2\mu_0\omega}\right)^{1/2}. \tag{18}$$

Therefore from Equations (9), (14)–(16), and (18), the power dissipated in the sphere due to its azimuthal velocity is, through second order,

$$P_{\text{sphere}}(v_\varphi) = \frac{\pi^3\sqrt{2}}{64}\left(\frac{\sigma}{\mu_0}\right)^{1/2} \times \omega^{3/2}r_o^4\left(\frac{R_p}{a}\right)^6 f(g_l^m, h_l^m), \tag{19}$$

where

$$f(g_l^m, h_l^m) = 5[(g_1^1)^2 + (h_1^1)^2] + (R_p/a)^2\{3[(g_2^1)^2 + (h_2^1)^2] + 39[(g_2^2)^2 + (h_2^2)^2]\}, \tag{20}$$

and we have averaged the products of the trigonometric functions of φ_o over 2π. The dissipation in Equation (19), and

resulting orbital evolution, is independent of the secondary's eccentricity. It is larger by a factor $\sim(r_o/\delta)^2$ than the corresponding induction heating (Chyba et al. 2021). For a satellite with an Fe or Fe–FeS core of radius $r_o \sim 10^3$ km, $(r_o/\delta)^2 \sim 10^8$.

We now examine ohmic heating that results from eccentric and inclined orbits.

3.2. Radial Velocities for Eccentric Orbits

Equation (6) allows the calculation of ohmic heating due to eccentric orbits for the general case; here we restrict our attention to the special case $\theta = \pi/2$ that is likely to be relevant in many applications. We include only the dipole term (Appendix A), which for many primaries will be the leading component of the magnetic field. Including more terms is straightforward. We have

$$\boldsymbol{v_r} \times \boldsymbol{B} = -v_r B_\varphi \hat{\theta} + v_r B_\theta \hat{\varphi}, \tag{21}$$

and with Equation (5) we calculate for the paths of cases (a)–(c) of Section 3.1:

$$\begin{aligned}\varepsilon(e \neq 0) &= \oint_{\tilde{C}_a} r v_r(-B_\varphi d\theta + B_\theta \sin\theta d\varphi) \\ &\approx -\frac{\pi^2}{2} ne\sqrt{1-e^2}\, r_o^2 \left(\frac{R_p}{a}\right)^3 g_1^0 \sin f,\end{aligned} \tag{22}$$

with an identical contribution from integrating around C_b, and zero contribution from the integral around C_c. Since $\sin^2 f$ averages to $1/2$ around the orbit, and with $r_o \gg \delta$ once again, by Equations (9) and (18), we have

$$\begin{aligned}P_{\text{sphere}}(e \neq 0) = &\frac{\pi^3\sqrt{2}}{8}\left(\frac{\sigma}{\mu_0}\right)^{1/2} \\ &\times n^{3/2} e^2 (1-e^2) r_o^4 \left(\frac{R_p}{a}\right)^6 (g_1^0)^2.\end{aligned} \tag{23}$$

Note that even in K, the relevant angular velocity here, including in the definition of δ, is n, not ω, since v_r depends on n and is independent of Ω. (For intuition, imagine a primary with an axisymmetric field, in which case it is clear that the frequency relevant to the skin depth in the secondary is independent of the rotation of the primary.)

3.3. Velocities Out of the Plane for Inclined Orbits

Finally, we use Equation (7) to calculate dissipation resulting from the secondary's out-of-plane velocity in an inclined orbit. Neptune's moon Triton, with its inclination of 157°.3 (National Space Science Data Center 2020) is our solar system's model for such a case. We display the result for the dipole term only; higher-order terms are readily calculated. We have

$$\boldsymbol{v_\theta} \times \boldsymbol{B} = v_\theta B_\varphi \hat{r} - v_\theta B_r \hat{\varphi}, \tag{24}$$

and with Equation (5) we calculate for the paths of cases (a)–(c) in Section 3.1:

$$\begin{aligned}\varepsilon(i \neq 0) &= \oint_{\tilde{C}_a} v_\theta (B_\varphi dr - B_r r \sin\theta d\varphi) \\ &\approx \pi n \sin i\, r_o^2 \left(\frac{R_p}{a}\right)^3 g_1^0,\end{aligned} \tag{25}$$

with an identical contribution from integrating around C_b, and zero contribution from C_c. With $r_o \gg \delta$ (again defined with n, not ω), we have

$$\begin{aligned}P_{\text{sphere}}(i \neq 0) = &\pi\sqrt{2}\left(\frac{\sigma}{\mu_0}\right)^{1/2} \\ &\times n^{3/2} \sin^2 i\, r_o^4 \left(\frac{R_p}{a}\right)^6 (g_1^0)^2.\end{aligned} \tag{26}$$

4. Ohmic Heating for Conducting Spherical Shells

We now present equations for ohmic heating for the three cases in Sections 3.1, 3.2, and 3.3, except for conducting spherical shells (such as magma or liquid water oceans) rather than solid spheres. We consider shells of outer radius r_o and thickness h.

4.1. Thick Shells ($h \gg \delta$)

For a shell with $h \gg \delta$, the equations for R, L, and Z are identical to those for the conducting sphere, so that Equation (18) continues to hold (Chyba et al. 2021). Therefore, Equations (19), (22), and (25) are identical for conducting spheres and spherical shells.

4.2. Thin Shells ($h \ll \delta$)

In the opposite limit where $h \ll \delta$, we have (Chyba et al. 2021)

$$R_{\text{shell}} = \frac{\pi}{2\sigma h} \quad \text{and} \quad L_{\text{shell}} = \frac{\pi\sqrt{3}}{8}\mu_0 r_o, \tag{27}$$

so that by Equation (10)

$$\frac{R}{Z^2} = \frac{2\sigma h}{\pi}\left(1 + \frac{3h^2 r_o^2}{4\delta^4}\right)^{-1}. \tag{28}$$

Therefore from Equations (9), (14)–(16), and (28), the power dissipated in the shell due to its azimuthal velocity is

$$\begin{aligned}P_{\text{shell}}^{h\ll\delta}(v_\varphi) = &\frac{\pi^3}{16}\sigma\omega^2 r_o^4 h\left(1 + \frac{3h^2 r_o^2}{4\delta^4}\right)^{-1} \\ &\times \left(\frac{R_p}{a}\right)^6 f(g_l^m, h_l^m),\end{aligned} \tag{29}$$

with $f(g_l^m, h_l^m)$ given by Equation (20). Power dissipation in the shell due to the radial velocity in an elliptical orbit is

$$\begin{aligned}P_{\text{shell}}^{h\ll\delta}(e \neq 0) = &\frac{\pi^3}{4}\sigma n^2 e^2 (1-e^2) \\ &\times h r_o^4 \left(1 + \frac{3h^2 r_o^2}{4\delta^4}\right)^{-1} \left(\frac{R_p}{a}\right)^6 (g_1^0)^2;\end{aligned} \tag{30}$$

and dissipation due to the $\hat{\theta}$-velocity in an inclined orbit is

$$\begin{aligned}P_{\text{shell}}^{h\ll\delta}(i \neq 0) = &2\pi\sigma n^2 \sin^2 i\, r_o^4 h \\ &\times \left(1 + \frac{3h^2 r_o^2}{4\delta^4}\right)^{-1} \left(\frac{R_p}{a}\right)^6 (g_1^0)^2.\end{aligned} \tag{31}$$

Equations (29)–(31) are identical to within a small numerical factor to those found via a simple induction-heating model,

which was shown to generate negligible heating for satellites in our current solar system (Chyba et al. 2021). In the limit where $\delta \gg h$, $\boldsymbol{B}^{m\neq 0}$ is not attenuated by the conducting shell, so that in K we have $\partial \boldsymbol{B}/\partial t = \boldsymbol{0}$ regardless of the secondary's orbital motion.

5. Example: Ohmic Heating of Io

We illustrate the heating mechanism described here using two different interior models for Jupiter's moon Io. These will also serve as illustrative examples for ohmic heating of possible moons in extrasolar systems. A more comprehensive application of this model to other solar system satellites will be presented elsewhere. Io, a satellite of radius 1821.5 km, orbits a rotating Jupiter ($\Omega = 1.76 \times 10^{-4}$ s^{-1}) with $n = 4.11 \times 10^{-5}$ s^{-1}, $\omega = 1.35 \times 10^{-4}$ s^{-1}, $(R_p/a) = 0.169$, $e = 0.004$, and $i = 0.^{\circ}04$ (National Space Science Data Center 2020). Jupiter's magnetic field has Schmidt coefficients $g_1^0 = 410{,}244.7$ nT, $g_1^1 = -71{,}498.3]$ nT, $h_1^1 = 21{,}330.5$ nT, $g_2^1 = -56{,}835.8$ nT, $h_2^1 = -42{,}027.3$ nT, $g_2^2 = 48{,}689.5$ nT, and $h_2^2 = 19{,}353.2$ nT (Connerney et al. 2018). We first use one possible interior model for Io (Schubert et al. 1986; Davies 2007) that takes it to have an Fe–FeS core of radius $r_o = 950$ km with $\sigma = 1 \times 10^6$ S m^{-1}, appropriate to FeS at temperature 1900 K and pressure 6 GPa (Li et al. 2007), approximately correct for the pressure and temperature at the upper boundary of Io's core. Liquid Fe at these pressures also has $\sigma \approx 1 \times 10^6$ S m^{-1} (Silber et al. 2018). (An alternate end-member Fe-core model for Io (Davies 2007) would have $r_o = 650$ km.) With these values, $\boldsymbol{B}$ has a skin depth $\delta = (2/\sigma\omega\mu_0)^{1/2} = 110$ m into the core. Io's metallic core is overlain by a rock mantle of outer radius 1791 km and thickness $h = 840$ km (Davies 2007). It is unclear whether or not this mantle contains a liquid magma ocean (Khurana et al. 2011; Bierson & Nimmo 2016; Blöcker et al. 2018).

The electrical conductivity of the mantle is unknown (e.g., Colburn 1980; Khurana et al. 2011), and depends inter alia on the uncertain presence of the magma ocean. First consider the case where the conductivity of Io's mantle is $<10^{-2}$ S m^{-1}, too low to shield Io's core from Jupiter's time-varying $\boldsymbol{B}$ field. (Even were Io to have a fully or partially shielded metallic core at present, our mechanism could be of interest to an early Io prior to entering the Laplace resonance; Yoder 1979; Greenberg 1982, or to a variety of other moons or exomoons.) In this model, Io's Fe–FeS core ($r_o = 950$ km) is ohmically heated according to Equation (19), which gives $P_{\rm Io}^{\rm core}(v_\varphi) = 570$ GW. This is greater than the expected radiogenic heating for Io, assuming chondritic composition (Cassen et al. 1982). The ohmic heating is concentrated in the outer 100 m of Io's Fe–FeS core, with a power density 4.6×10^{-4} W m^{-3}, rather than being distributed throughout the lithosphere as for radiogenic heating. These results could affect heating profiles for interior models of Io (e.g., Bierson & Nimmo 2016), and resulting physical conclusions. Six hundred gigawatts of ohmic heating is <1% of Io's observed heat flow 1×10^{14} W, attributed to tidal dissipation (Lainey et al. 2009; Veeder et al. 2012).

Early Io would have rapidly become spin locked (on a timescale $\sim 10^3$ yr) and its orbit circularized (on a timescale $\sim 10^7$ yr) (Murray & Dermott 1999), after which tidal dissipation in Io ceased until Io entered into resonance with Europa (Yoder 1979), unless this resonance were somehow primordial (Greenberg 1982). But even after spin-locking and orbit circularization, ohmic heating would have persisted and could have been high: if Io were closer to Jupiter in the past, ohmic heating would have increased like $a^{-6}(\Omega - n)^{3/2}$. For example, a spin-locked Io at $3R_p$ with $e = 0$ would have experienced 15,000 GW of ohmic heating, dissipation that could be important to understanding Io's thermal and orbital history.

By contrast, consider a second interior model in which a more conducting magma mantle shields the Fe–FeS core due to the skin effect, i.e., a mantle for which $h \gg \delta$. In this case, Equation (19) again applies, with r_o the radius of the mantle. The conductivity of the mantle in this scenario is uncertain but for illustration we take it to be at the upper end of plausible ultramafic rock melts, $\sigma = 5$ S m^{-1} (Khurana et al. 2011). This value is about the same as that for a salty ocean (say on a Europa-like world). Then $P_{\rm Io}^{\rm mantle}(v_\varphi) = 15$ GW, much smaller than radiogenic heating.

6. Orbital Evolution

Had Io experienced its current possible 570 GW of ohmic heating throughout the history of the solar system, a total of 1×10^{29} J would have been dissipated in Io over that time, ~1% of Io's current orbital energy. Nevertheless, ohmic heating might have been important to Io's orbital history, especially if Jupiter's tidal quality factor Q_J was large. As just noted, in an elegant scenario for the evolution of Io, Europa, and Ganymede into their three-body Laplace resonance (Yoder 1979), early Io rapidly despun, its orbit circularized, and its tidal dissipation ceased. Io then evolved outward in its orbit due to a Jovian off-radial tidal bulge raised by Io. The resulting torque expanded Io's orbit faster than Europa's. Once Io entered into resonance, its eccentricity increased, which in turn drove (and drives) tidal heating, possibly runaway melting, and perhaps now even inward migration out of the resonance (Lainey et al. 2009). The characteristic timescale τ_p for orbital expansion due to torques from planet tides (tides raised on Jupiter by Io) is just (e.g., Chyba et al. 1989; Murray & Dermott 1999)

$$\tau_p = \frac{2}{39}\left(\frac{M_p}{G}\right)^{1/2}\left(\frac{Q_p}{k_p}\right)\frac{a^{13/2}}{m_s R_p^5}, \tag{32}$$

where in our example M_p is Jupiter's mass, m_s is the mass of Io, and we take $k_p = 1/2$ to be the fluid Love number for Jupiter (Peale et al. 1979; Yoder 1979).

As with tidal dissipation in the secondary, ohmic dissipation comes out of the secondary's orbital energy $E_{\rm orb}$, so acts to decrease the semimajor axis of the orbit according to

$$P_{\rm sphere}(v_\varphi) = \dot{E}_{\rm orb} = \frac{GM_p m_s}{2a^2}\dot{a}, \tag{33}$$

giving a timescale for orbital contraction due to ohmic dissipation,

$$\tau_{\rm ohm} \equiv \frac{a}{\dot{a}} = \frac{GM_p m_s}{2aP_{\rm sphere}(v_\varphi)}. \tag{34}$$

Using Equations (32), (34), and (19), we can compare the timescale τ_p for orbital expansion due to tides raised on the primary (in this case Jupiter), to the timescale $\tau_{\rm ohm}$ for orbital contraction due to ohmic dissipation in the secondary (in this

case Io), and find that

$$\frac{\tau_p}{\tau_{\rm ohm}} = \frac{\pi^3\sqrt{2}}{96}\left(\frac{\omega a}{G}\right)^{3/2}\left(\frac{\sigma}{\mu_0}\right)^{1/2} \times \left(\frac{r_o^2}{m_s}\right)^2\left(\frac{Q_p}{k_p}\right)\left(\frac{R_p^2}{M_p}\right)^{1/2} f(g_l^m, h_l^m), \quad (35)$$

with $f(g_l^m, h_l^m)$ from Equation (20). For larger a, orbital contraction due to ohmic dissipation in the secondary becomes increasingly important relative to orbital expansion due to tides on the primary. This sets a limit to how far out a secondary with ohmic dissipation in its core can migrate. This contrasts with the analogous ratio τ_p/τ_s, where τ_s is the timescale for orbital contraction due to tidal dissipation in the satellite: the ratio τ_p/τ_s is independent of a (Chyba et al. 1989).

For contemporary Io, $\tau_p/\tau_{\rm ohm} \approx 1 \times 10^{-7}\, Q_p$. Yoder (1979) argues that $2 \times 10^5 < Q_p < 2 \times 10^6$, consistent with other values derived from tidal evolution arguments that require the Galilean satellites not to have been pushed too far away from Jupiter over the age of the solar system, but to have been pushed enough to have entered into resonance (Goldreich & Soter 1966; Greenberg 1982). Some interior models of Jupiter suggest values of Q_p as large as 10^9 or higher (Greenberg 1982; Wu 2005); $Q_p \gtrsim 1 \times 10^7$ in Equation (35) would imply a contemporary Io with a contracting orbit due to ohmic dissipation alone. Such a world would migrate inward until the dependence in Equation (35) on $[(\Omega - n)a]^{3/2}$ brought contraction into balance with orbital expansion driven by Jupiter tides and migration came to a halt.

However, Lainey et al. (2009) have used astrometric observations of the Galilean moons to argue that Io is evolving inward due to tidal dissipation in Io, and find $Q_p/k_p = (1.102 \pm 0.203) \times 10^{-5}$ for Jupiter. For $k_p = 0.5$, this gives $Q_p = 4.5 \times 10^4$, in which case orbital evolution due to ohmic dissipation never dominates outward migration driven by tides on Jupiter.

Regardless of tidal dissipation in the primary, Equation (19) shows that inward orbital migration due to ohmic dissipation must stop when $n = \Omega$. One can imagine a system (perhaps early solar system or extrasolar) in which $\tau_p/\tau_{ohm} > 1$ in Equation (35). Then the secondary would migrate inward until it reached $a = [G(M_p + m_s)/\Omega^2]^{1/3}$, corresponding to $n = \Omega$. For Jupiter the corresponding Jovicentric distance of $2.2R_p$ is comparable to the Roche limit, so that secondaries might be (and could in the past have been) altogether lost. But for primaries with somewhat smaller values of Ω, the semimajor axis at which inward migration stops could lie well outside the Roche limit. However, if the secondary were heated due to ohmic dissipation in its core sufficient to form a thick and conductive ($h \gg \delta$) magma or liquid water ocean, the core would then become largely shielded from $\boldsymbol{B}^{m\neq 0}$, causing heating to drop by as much as several orders of magnitude, leading the secondary to turn around in its migration (as $\tau_p/\tau_{\rm ohm} > 1$ in Equation (35) changes to $\tau_p/\tau_{\rm ohm} < 1$) and expand its orbit due to the subsequently dominant effects of torques from tides on the primary. Migration histories for secondaries, and implied limits for Q_p, are complicated by these potential histories. For secondaries such as Triton with substantial inclinations, Equation (25) means that $\tau_p/\tau_{\rm ohm}$ has a very different dependence on a than that found in Equation (35); we will explore this case elsewhere.

We thank P. J. Thomas and an anonymous referee for their reviews, and G. Z. McDermott for reference assistance. K.P.H. acknowledges support from the Jet Propulsion Laboratory, California Institute of Technology, under contract with NASA. C.F.C. acknowledges support from Princeton University.

Appendix A
Axisymmetric Magnetic Flux Density through Second Order

We make such frequent use of the magnetic flux density ($\boldsymbol{B}$) components of the primary through second order that we display them here in the appendix, rather than ask the reader to derive them from the magnetic potential U (with $\boldsymbol{B} = -\boldsymbol{\nabla} U$) whenever they are needed. We use the usual model (e.g., Parkinson 1983; Merrill et al. 1998) with U written in terms of Schmidt-normalized associated Legendre polynomials with coefficients g_l^m and h_l^m of degree l and order m. Units are those of magnetic flux density.

The axisymmetric dipole (the lowest-order axisymmetric field) then has the components

$$B_r^{1,0} = 2(R_p/r)^3 g_1^0 \cos\theta, \quad (A1a)$$

$$B_\theta^{1,0} = (R_p/r)^3 g_1^0 \sin\theta, \quad (A1b)$$

$$B_\varphi^{1,0} = 0, \quad (A1c)$$

where R_p is the appropriate reference radius for the primary, and the superscript "1, 0" labels these as components of the dipole field.

The axisymmetric quadrupole has components

$$B_r^{2,0} = \frac{3}{2}(R_p/r)^4 g_2^0 (3\cos^2\theta - 1), \quad (A2a)$$

$$B_\theta^{2,0} = 3(R_p/r)^4 g_2^0 \cos\theta \sin\theta, \quad (A2b)$$

$$B_\varphi^{2,0} = 0. \quad (A2c)$$

Obviously $\boldsymbol{B^{1,0}}$ and $\boldsymbol{B^{2,0}}$ have no φ dependence.

Appendix B
Nonaxisymmetric Magnetic Flux Density through Second Order

By Equation (4) all g_l^0 terms contribute $\mathbf{0}$ to Equation (2). The first-order terms of degree one, g_1^1 and h_1^1, are typically the leading off-axis terms, corresponding to orthogonal dipoles lying in the equatorial plane. They are given by

$$B_r^{1,1} = 2(R_p/r)^3(g_1^1\cos\varphi + h_1^1\sin\varphi)\sin\theta, \quad (B1a)$$

$$B_\theta^{1,1} = -(R_p/r)^3(g_1^1\cos\varphi + h_1^1\sin\varphi)\cos\theta, \quad (B1b)$$

$$B_\varphi^{1,1} = (R_p/r)^3(g_1^1\sin\varphi - h_1^1\cos\varphi). \quad (B1c)$$

The components of order 2, degree 1 are

$$B_r^{2,1} = 3\sqrt{3}\,(R_p/r)^4 \times (g_2^1\cos\varphi + h_2^1\sin\varphi)\cos\theta\sin\theta, \quad (B2a)$$

$$B_\theta^{2,1} = \sqrt{3}\,(R_p/r)^4 \times (g_2^1\cos\varphi + h_2^1\sin\varphi)(\sin^2\theta - \cos^2\theta), \quad (B2b)$$

$$B_\varphi^{2,1} = \sqrt{3}\,(R_p/r)^4(g_2^1\sin\varphi - h_2^1\cos\varphi)\cos\theta. \quad (B2c)$$

Finally, the order 2, degree 2 components are

$$B_r^{2,2} = \frac{3\sqrt{3}}{2}(R_p/r)^4 \times (g_2^2 \cos 2\varphi + h_2^2 \sin 2\varphi)\sin^2\theta, \quad \text{(B3a)}$$

$$B_\theta^{2,2} = -\sqrt{3}\,(R_p/r)^4 \times [(g_2^2 \cos 2\varphi + h_2^2 \sin 2\varphi)\cos\theta \sin\theta, \quad \text{(B3b)}$$

$$B_\varphi^{2,2} = \sqrt{3}\,(R_p/r)^4 (g_2^2 \sin 2\varphi - h_2^2 \cos 2\varphi)\sin\theta. \quad \text{(B3c)}$$

Appendix C
Example emf Calculation

Here we show explicitly how the path in Figure 1(a) allows the calculation of the Equation (14) line integral. The segments in Figure 1(a) lie in the $\hat{\theta}$ and $\hat{\varphi}$ directions, so by Equation (12), only the two segments in the $\hat{\theta}$ direction contribute to the integral. By Equation (4), $B_r^{1,0}$ and $B_r^{2,0}$ contribute nothing. To a sufficient approximation, we take $r = a$ (the choice $r = a + \rho_o$, say, introduces terms of higher order in ρ_o/a). Through second order, Equation (14) then becomes

$$\varepsilon = \omega a^2 \left[\int_{\pi/2+\rho_o/a}^{\pi/2-\rho_o/a} d\theta\, \sin\theta (B_r^{1,1} + B_r^{2,1} + B_r^{2,2})_{\varphi=\varphi_0-\rho_o/a} + \int_{\pi/2-\rho_o/a}^{\pi/2+\rho_o/a} d\theta\, \sin\theta (B_r^{1,1} + B_r^{2,1} + B_r^{2,2})_{\varphi=\varphi_0+\rho_o/a} \right]. \quad \text{(C1)}$$

By Equation (B2a), the $B_r^{2,1}$ terms integrate to zero. After integration, the use of sum and difference formulas and small-angle approximations for the trigonometric functions gives the result in Equation (14). Equations (15) and (16) are calculated analogously, though all four segments contribute to the integral in Equation (16). In Equation (15), to a sufficient approximation we take $\theta = \pi/2$; in Equation (16) we take $\varphi = \varphi_0$.

ORCID iDs

Christopher F. Chyba https://orcid.org/0000-0002-6757-4522
Kevin P. Hand https://orcid.org/0000-0002-3225-9426

References

Auchmann, B., Kurz, S., & Russenschuck, S. 2014, ITM, 50, 7025404
Bierson, C. J., & Nimmo, F. 2016, JGRE, 121, 2211
Blöcker, A., Saur, J., Roth, L., & Strobel, D. F. 2018, JGRA, 123, 9286
Campbell, W. H. 2003, Introduction to Geomagnetic Fields (Cambridge: Cambridge Univ. Press)
Cassen, P. M., Peale, S. J., & Reynolds, R. T. 1982, in Satellites of Jupiter, ed. D. Morrison (Tucson, ARI: Univ. Arizona Press), 93
Christensen, U. R., Dougherty, M. K., & Khurana, K. 2019, in Saturn in the 21st Century, ed. K. H. Baines et al. (Cambridge: Cambridge Univ. Press), 69
Chyba, C. F., & Hand, K. P. 2016, PhRvP, 6, 014017
Chyba, C. F., & Hand, K. P. 2020, PhRvP, 13, 028002
Chyba, C. F., Hand, K. P., & Thomas, P. J. 2015, AmJPh, 83, 72
Chyba, C. F., Hand, K. P., & Thomas, P. J. 2021, Icar, 360, 114360
Chyba, C. F., Jankowski, D. G., & Nicholson, P. D. 1989, A&A, 219, L23
Colburn, D. S. 1980, JGR, 85, 7257
Colburn, D. S., & Reynolds, R. T. 1985, Icar, 63, 39
Connerney, J. E. P., Kotsiaros, S., Oliverson, R. J., et al. 2018, GeoRL, 45, 2590
Davies, A. G. 2007, Volcanism on Io (Cambridge: Cambridge Univ. Press)
Drobyshevski, E. M. 1979, Natur, 282, 811
Faraday, M. 1832, RSPT, 122, 125
Goertz, C. 1980, JGR, 85, 2949
Goldreich, P., & Lynden-Bell, D. 1969, ApJ, 156, 59
Goldreich, P., & Soter, S. 1966, Icar, 5, 375
Greenberg, R. 1982, in Satellites of Jupiter, ed. D. Morrison (Tucson, ARI: Univ. Arizona Press), 65
Gutmann, R. J., & Borrego, J. M. 1974, ITAP, 22, 635
Hand, K. P., Khurana, K., & Chyba, C. F. 2011, JGR, 116, E04010
Khurana, K. K., Jia, X., Kivelson, M. G., et al. 2011, Sci, 332, 6034
Khurana, K. K., Kivelson, M. G., Stevenson, D. J., et al. 1998, Natur, 395, 777
Kislyakova, K. G., Noack, L., Johnstone, C. P., et al. 2017, NatAs, 1, 878
Laine, R. O., & Lin, D. N. C. 2012, ApJ, 745, 2
Laine, R. O., Lin, D. N. C., & Shawfeng, D. 2008, ApJ, 685, 521
Lainey, V., Arlot, J., Özgür, K., & Van Hoolst, T. 2009, Natur, 459, 957
Li, M., Gao, C.-X., Zhang, D.-M., et al. 2007, ChPhL, 24, 54
Lorrain, P., McTavish, J., & Lorrain, F. 1998, EJPh, 19, 451
Merrill, R. T., McElhinny, M. W., & McFadden, P. L. 1998, The Magnetic Field of the Earth (New York: Academic)
Munley, F. 2004, AmJPh, 72, 1478
Murray, C. D., & Dermott, S. F. 1999, Solar System Dynamics (Cambridge: Cambridge Univ. Press)
National Space Science Data Center 2020, Jupiter Fact Sheet, http://nssdc.gsfc.nasa.gov/planetary/factsheet/jupiterfact.html
Parkinson, W. D. 1983, Introduction to Geomagnetism (Edinburgh: Scottish Academic Press)
Peale, S. J., Cassen, P., & Reynolds, R. T. 1979, Sci, 203, 892
Piddington, J. H., & Drake, J. K. 1968, Natur, 217, 935
Redžić, D. V. 2004, EJPh, 25, 623
Reynolds, R. T., Squyres, S. Q., Colburn, D. S., & McKay, C. P. 1983, Icar, 56, 246
Roth, L., Saur, J., Retherford, K. D., et al. 2014, Sci, 343, 171
Russell, C. T., & Huddleston, D. E. 2000, AdSpR, 26, 1665
Saur, J., Neubauer, F. M., Connerney, J. E. P., Zarka, P., & Kivelson, M. G. 2004, in Jupiter: The Planet, Satellites and Magnetosphere, ed. F. Bagenal, T. E. Dowling, & W. B. McKinnon (Cambridge: Cambridge Univ. Press), 561
Scanlon, P. J., Henriksen, R. N., & Allen, J. R. 1969, AmJPh, 37, 698
Schubert, G., Spohn, T., & Reynolds, R. T. 1986, in Satellites, ed. J. A. Burns & M. S. Matthews (Tucson, AZ: Univ. Arizona Press), 224
Silber, R. E., Secco, R. A., Yong, W., & Littleton, J. A. H. 2018, NatSR, 8, 10758
Simonelli, D. P. 1983, Icar, 54, 524
Sonnet, C. P., Colburn, D. S., Schwartz, K., & Keil, K. 1970, Ap&SS, 7, 446
Sparks, W. B., Hand, K. P., McGrath, M. A., et al. 2016, ApJ, 829, 121
Veeder, G. J., Davies, A. G., Matson, D. L., et al. 2012, Icar, 219, 701
Wouch, G., & Lord, A. E. 1978, AmJPh, 46, 464
Wu, Y. 2005, ApJ, 635, 688
Yoder, C. F. 1979, Natur, 279, 767